# Steep Cliffs and Saturated Exponents in Three-Dimensional Scalar Turbulence

Kartik P. Iyer, Jörg Schumacher, Katepalli R. Sreenivasan, and P. K. Yeung

Phys. Rev. Lett. **121**, 264501 — Published 28 December 2018

DOI: 10.1103/PhysRevLett.121.264501

# Steep cliffs and saturated exponents in three dimensional scalar turbulence

Kartik P. Iyer,[1,*] Jörg Schumacher,[1,2] Katepalli R. Sreenivasan,[1,3] and P K Yeung[4]

[1] *Tandon School of Engineering, New York University, New York, NY 11201, USA*
[2] *Institut für Thermo- und Fluiddynamik, Technische Universität Ilmenau, Postfach 100565, D-98684 Ilmenau, Germany*
[3] *Department of Physics and the Courant Institute of Mathematical Sciences, New York, NY 10012, USA*
[4] *School of Aerospace and Mechanical Engineering, Georgia Institute of Technology, Atlanta, GA 30332, USA*

(Dated: November 9, 2018)

The intermittency of a passive scalar advected by three-dimensional Navier-Stokes turbulence at a Taylor-scale Reynolds number of 650 is studied using direct numerical simulations on a $4096^3$ grid; the Schmidt number is unity. By measuring scalar increment moments of high orders, while ensuring statistical convergence, we provide unambiguous evidence that the scaling exponents saturate to 1.2 for moment order beyond about 12, indicating that scalar intermittency is dominated by the most singular shock-like cliffs in the scalar field. We show that the fractal dimension of the spatial support of steep cliffs is about 1.8, whose sum with the saturation exponent value of 1.2 adds up to the space dimension of 3, thus demonstrating a deep connection between the geometry and statistics in turbulent scalar mixing. The anomaly for the fourth and sixth order moments is comparable to that in the Kraichnan model for the roughness exponent of 4/3.

The mixing of a substance in a complex turbulent flow is a generic and fundamental problem which serves as a paradigm for many processes in nature and technology [1–5]. The basic characteristic of such turbulent systems is intermittency, manifested as intense and sporadic fluctuations of the small scales, which are not captured by classical mean field theories [6, 7]. Two important examples of intermittent systems are three-dimensional (3D) Navier-Stokes (NS) turbulence [8, 9] and 3D scalar turbulence [10, 11]—a short phrase for passive scalars mixed by NS turbulence.

Scalar turbulence provides a clear example of a generic feature of nonlinear multiscale phenomena, namely the connection between the multifractal scaling of statistical moments of the physical quantity or field under consideration to the geometric properties of the developing coherent structures. This intimate connection extends beyond fluid mechanics and can be found in various other fields of physics and beyond, such as in fracture mechanics of solids [12], nonlinear fiber optics [13], and bitcoin markets [14]. In all such multifractal statistical processes, quasi-discontinuous features characterized by steep *cliffs* or *fronts* abound, for instance, see Fig. 1. In the context of 3D turbulence, the influence of such cliffs on scalar intermittency has remained an open question.

In the related problems of Burgers turbulence [15–17] and the Kraichnan model [18] for a scalar advected by a synthetic velocity field with no temporal memory, much progress has been made on this particular subject [19–25]. However, the finite-time correlations of the advecting 3D NS turbulence has impeded theoretical progress, with the high spatial and temporal resolution requirements imposing considerable strain on empirical work. A large number of experimental and numerical efforts continue to be made on understanding scalar intermittency [26–34], but the connection between the intermittent statistics and the spatial geometry in 3D scalar mixing, has eluded a clear demonstration.

In this Letter, we report the precise quantification of small-scale intermittency of a statistically stationary scalar field, advected by 3D isotropic NS turbulence using direct numerical simulations (DNS). We connect the statistical footprints of the well-mixed scalar regions known as *ramps* [35–41], to the steep cliff regions. The scaling exponents $\zeta_p^\theta$ of the scalar correlations, which will be defined further below, saturate for moment orders above about 12, to a constant $\zeta_\infty^\theta$ confirming that the almost-shock-like steep scalar fronts characterize scalar intermittency in 3D NS turbulence. We will also show that the spatial support of the cliffs with a fractal dimension of $D_F = 1.8$ combines with the saturated scaling exponent $\zeta_\infty^\theta$ to the space dimension, yielding the result $\zeta_\infty^\theta + D_F = 3$, where 3 is the space dimension, thus demonstrating the intimate link between the geometry and statistics in turbulent passive scalar mixing.

We use data from pseudo-spectral DNS of isotropic turbulence, computed using $4096^3$ mesh points in a periodic box of size $L$. A statistically steady state was obtained by forcing the low Fourier modes of the velocity field [42]. The Taylor-scale Reynolds number $R_\lambda = 650$, the Schmidt number, $Sc = 1$, and the Taylor-scale Péclet number $Pe_\lambda \equiv R_\lambda Sc = 650$. The passive scalar ($\Theta$) is evolved using the diffusion-advection equation in the presence of a uniform mean gradient $\mathbf{G} \equiv (G, 0, 0)$ along the $x$-direction, where $G \neq 0$ is a constant, such that $\Theta = \theta + Gx$, $\theta$ here is the scalar fluctuation. The grid resolution $\Delta/\eta_K = 1.1$, $\Delta$ being the grid spacing and $\eta_K$ the Kolmogorov length scale. The ratio of the magnitude of the largest gradient computed in the DNS to the largest gradient possible in the flow ($\theta_{\rm rms}/\eta_K \sim GL/\eta_K \sim R_\lambda^{3/2}$) is $\sim O(1)$, where $\theta_{\rm rms} \equiv \sqrt{\langle\theta^2\rangle}$ and $\langle\cdot\rangle$ denotes combined space-time averages, hence the numerical resolution is

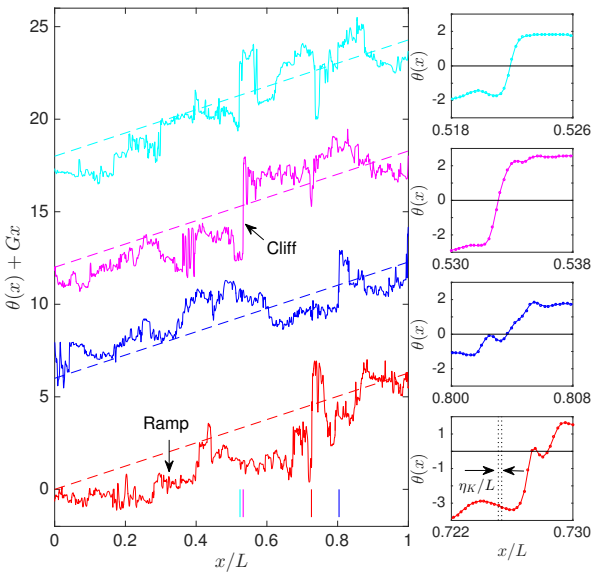


FIG. 1. Ramp-cliff structures in a scalar field, $\Theta \equiv \theta + Gx$, here $\theta$ is the scalar fluctuation and $(G, 0, 0)$ is the mean gradient, at $R_\lambda = 650$ and the Schmidt number $Sc \equiv \nu/D = 1$, where $\nu$ is the kinematic viscosity of the fluid and $D$ is the scalar diffusivity. $L$ is the size of the computational cube in one direction. The main figure to the left plots four 1D profiles of $\Theta$ in the $x$-direction, along which the mean gradient is imposed. Examples for ramps and cliffs are indicated by arrows as well as the mean scalar concentration profile (dashed lines). Profiles are shifted in steps of 5 units with respect to each other for clarity. The vertical solid lines indicate the spatial positions for the magnifications of the scalar fluctuation profiles plotted to the right. Grid resolution and Kolmogorov length $\eta_K$ are indicated.

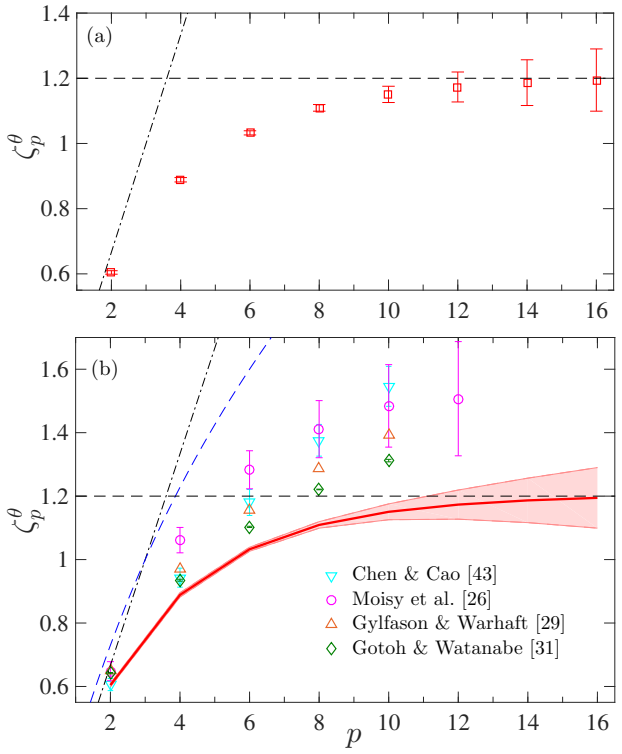


FIG. 2. Scalar increment exponent $\zeta_p^\theta$ *vs.* moment order $p$. (a) present DNS: $Pe_\lambda = 650$: dashed line at saturation exponent, $\zeta_\infty^\theta = 1.2$. Error bars indicate 95% confidence interval. (b) Comparison of present DNS (shaded region) with previous results: ($\triangledown$) $Pe_\lambda = 220$ [47]; ($\bigcirc$) $Pe_\lambda = 280$ [29]; ($\triangle$) $Pe_\lambda = 396$ [32]; ($\Diamond$) $Pe_\lambda = 580$ [34]. Dash-dotted line shows normal scaling $\zeta_p^\theta = p/3$; dashed line is the model of Ref. [28].

adequate to resolve the largest scalar gradients. We have used 21 temporal snapshots over 10 eddy turnover times, with each snapshot rotated over 146 angular directions to extract the isotropic statistics of the anisotropic scalar field. In total, we have used 210 trillion data samples to obtain the results. For details on the exact laws of the velocity and mixed velocity-scalar statistics and statistical convergence tests on the data, we refer to the supplemental information (SI) and Refs. [43–45].

The scalar signal organizes itself into conspicuous patterns as shown in Fig. 1, consisting of two distinctive features: (i) ramp regions where the total scalar gradient $\nabla\theta + \mathbf{G}$ is almost zero; and (ii) high gradient cliffs which are interspersed between ramps. The small figures on the right demonstrate clearly that the scalar increment, $\delta_r\theta \equiv \theta(\mathbf{x}+\mathbf{r}) - \theta(\mathbf{x})$, can jump by the order $GL$ over $r \equiv |\mathbf{r}|$ that is just a few multiples of the Kolmogorov scale $\eta_K$ (which is also the smallest dynamically significant scale in the scalar field). The ramp-cliff structure are connected to the mean scalar gradient in the present DNS, and are known to cause the breakdown of local isotropy in the scalar field [10]. The cliffs are caused by the action of large scales in the scalar field, even in the absence of a mean gradient [10, 46]. The generic existence of scalar cliffs in turbulence suggests that these local spatial barriers to scalar mixing have a significant impact on scalar intermittency.

In order to assess scalar intermittency, we define the $p$th order scalar structure function, $S_\theta^p(\mathbf{r}) \equiv \langle(\delta_r\theta)^p\rangle$. Due to the anisotropic mean scalar gradient, $S_\theta^p(\mathbf{r})$ depends on the separation vector $\mathbf{r}$, however, the isotropic sector $\langle(\delta_r\theta)^p\rangle_0$ extracted from the SO(3) decomposition [48, 49] of $S_\theta^p(\mathbf{r})$, depends solely on the separation distance, $r$ [50]. In the inertial range, $\eta_K \ll r \ll \ell$, where $\ell$ is the macro-scale, $30 \le r/\eta_K \le 300$, $\langle(\delta_r\theta)^p\rangle_0$ follow power laws, $\langle(\delta_r\theta)^p\rangle_0 \sim r^{\zeta_p^\theta}$, where $\zeta_p^\theta$ denote the $p$th order exponents (see SI for details). The higher order exponents are determined using extended self-similarity (ESS) [51], by plotting $\langle(\delta_r\theta)^p\rangle_0$ against $\langle(\delta_r\theta)^2\rangle_0$ for $p > 2$. We have verified that estimating $\zeta_p^\theta$ using local slopes, e.g. [34], or compensated structure functions, e.g. [29], yield results consistent with the ESS results.

The scaling exponents $\zeta_p^\theta$ are plotted against moment order $p$ at $Pe_\lambda = 650$ in Fig. 2(a). The exponents saturate to $\zeta_\infty^\theta = 1.2$, indicated by the horizontal line, for $p \ge 12$. This is the clearest indication that the scalar fluctuations are limited in magnitude only by the largest allowable

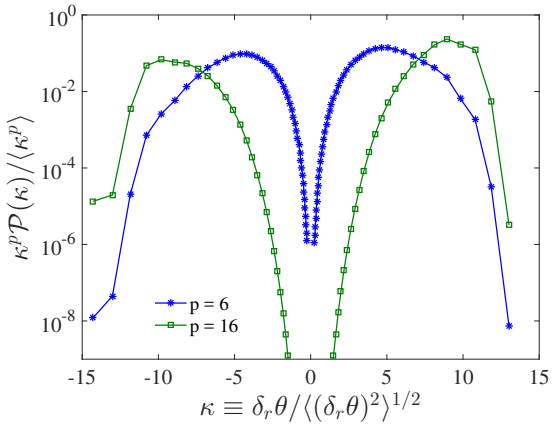


FIG. 3. Integrands of scalar increment moments ($\mathcal{P}(\cdot)$ denotes PDF of $(\cdot)$) as functions of scalar increments, for orders 6 and 16 at $r/\eta_K = 55$ (lower end of the inertial range), on lin-log scales; moments of orders up to 20 converge as well and confirm the saturation of exponents but are not shown here. The integrands are normalized by respective moments such that the area under each curve is unity.

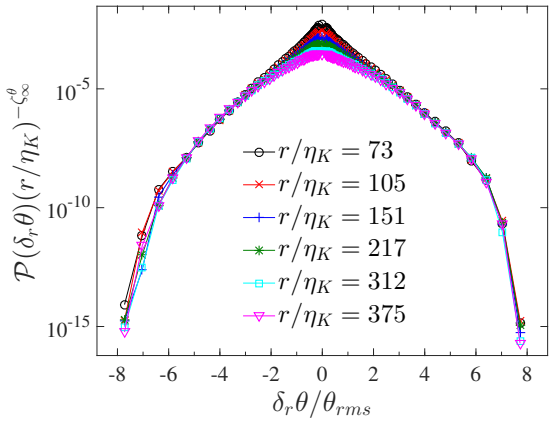


FIG. 4. PDF of scalar increments across the inertial range, multiplied by $r^{-\zeta^\theta_\infty}$, where $\zeta^\theta_\infty$ is the saturation exponent (Fig. 2). The PDF tails collapse, confirming saturation of exponents.

gradients in the field (largest temperature difference divided by the smallest length scale). The $\zeta^\theta_\infty = 1.2$ curve intersects the normal scaling curve at $p = 3.6$. In some sense, it is possible that this represents the situation for infinitely large $Pe_\lambda$. Figure 2(b) compares the present exponents with previous, lower $Pe_\lambda$, results. While our data robustly confirm that the exponents saturate, it is hard to reach a similar unambiguous conclusion from the previous results in the literature [29–32, 34, 47, 52].

The statistical convergence of the moments of order $p$ up to 20 was confirmed by the rapid decay of the moment integrands, $(\delta_r\theta)^p\mathcal{P}(\delta_r\theta)$, where $\mathcal{P}$ denotes the probability density function (PDF). The integrands of moment orders 6 and 16 are shown in Fig. 3, each for $r$ in the low end of the inertial range. The integrands peak before the tail contributions decay, ensuring statistical convergence

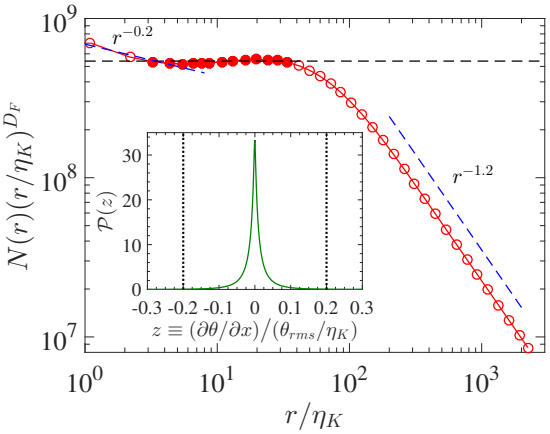


FIG. 5. Log-log plot of the number $N(r)$ of cubes of side $r$ containing the steepest fronts *vs.* size $r$. The ordinate is compensated by $r^{D_F}$, where $D_F = 1.8$ is the fractal co-dimension of the fronts. The plateau region (●) corresponds to the scaling $r^{-D_F}$, indicated by the horizontal dashed line. At the smallest and largest $r$, the dimension of the fronts is 2 (corresponding to flat fronts) and 3 (which is the Euclidean dimension of the flow), respectively. Inset shows the PDF of the normalized gradient $z$, $|z| > 0.2$ (dotted lines) is used to calculate $N(r)$.

of the moments. Saturation of exponents at higher orders implies that, for scalar jumps $|\delta_r\theta| \gtrsim \theta_{\rm rms}$, $\mathcal{P}(\delta_r\theta) \propto r^{\zeta^\theta_\infty}$, [23, 53]. Figure 4 verifies that this is indeed the case, with $\mathcal{P}(\delta_r\theta)r^{-\zeta^\theta_\infty}$ collapsing for $|\delta_r\theta| \geq 3\theta_{\rm rms}$, for all inertial separations. The inference is that the saturation of exponents arises because of the dominance of the high order moments by features that do not change with scale, suggesting that the gradients are of the order $\theta_{rms}/\eta_K$.

We now turn to quantifying the dimension of the spatial support of the cliffs where strong scalar gradients tend to concentrate in sharp fronts (Fig. 1). The dimension of such fronts is estimated by the spatial support of regions of the strongest gradients of $\mathcal{O}(\theta_{rms}/\eta_K)$ with cubes of edge size $r$, and counting their respective number $N(r)$ for different $r$. As shown in the inset of Fig. 5, gradients greater than 20% of $\theta_{rms}/\eta_K$ (marked by dotted lines) corresponding to $5\sqrt{\langle(\partial\theta/\partial x)^2\rangle}$, are used to determine $N(r)$. We chose the threshold of 20% as a good representative of gradients of the order $\theta_{rms}/\eta_K$ occurring with low probability (see inset to Fig. 5). [The use of a somewhat different threshold alters the scaling range in Fig. 5 but does not alter the dimension itself.] The plot of $N(r)$ *vs.* $r$ for such fronts shown in the main body of Fig. 5, is compensated by $r^{1.8}$ (see below for the rationale), and has three scaling regimes: (i) at the smallest scales, a slope of $-2$ which corresponds to flat fronts; (ii) at $r/\eta_K \in [4, 30]$, for which the slope from the least-squares fit is $D_F = 1.79 \pm 0.01$, corresponding to the spatial subset that supports the steep fronts in the scalar field; (iii) at the largest scales, the slope is $-3$ which corresponds to the Euclidean dimension of the flow. We

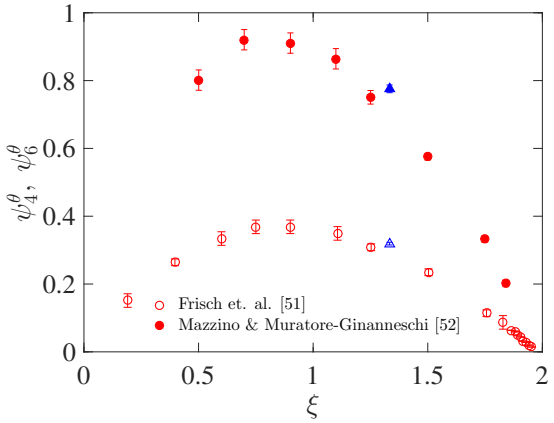


FIG. 6. Flatness anomaly ($\psi_4^\theta = 2\zeta_2^\theta - \zeta_4^\theta$) (open symbols) and hyper-flatness anomaly ($\psi_6^\theta = 3\zeta_2^\theta - \zeta_6^\theta$) (closed symbols) for the scalar *vs.* flow roughness $\xi$. Circles correspond to 3D Kraichnan model, (○) [54] and (●) [55], while triangles are for 3D NS flow at $Pe_\lambda = 650$, with the roughness parameter $\xi = 4/3$.

confirm, for the first time in 3D NS flows, that the saturation exponent $\zeta_\infty^\theta$ and the box counting dimension of the steep fronts $D_F$ are related to the space dimension, $d = 3$, as

$$\zeta_\infty^\theta + D_F = d\,. \tag{1}$$

The confirmation of this relation in Navier-Stokes turbulence is remarkable since it directly connects a property of the highly intermittent statistics of the scalar to the spatial geometry of mixing barriers in the flow. The geometrical features of the scalar cliffs shown here has interesting parallels beyond fluid turbulence, e.g. in fracture processes in solids, where a network of steep cliffs with a fractal dimension $D_F \approx 1.7$, detected on a fracture surface and related to the multifractal spectrum of height fluctuations, tends to saturate [12].

The anomaly in the passive scalar field advected by a 3D NS flow at high-$R_\lambda$ is comparable for orders 4 and 6 to that advected by the $\delta$-correlated 3D Kraichnan model [54, 55], as seen in Fig. 6 where we quantify the degree of anomaly of exponents against the roughness parameter of the flow (which varies between 0 and 2 for Kraichnan model and is 4/3 for NS turbulence). This observed agreement is plausible because, in a high-$R_\lambda$ NS flow, the small scales evolve with temporal rapidity, and the normalized exponents, $\psi_p^\theta \equiv (p/2)\zeta_2^\theta - \zeta_p^\theta$, approach the Kraichnan limit of a flow without memory. Scalar exponents for the Kraichnan model saturate at different values for different roughness parameters [23, 53], and the observed correspondence with the 3D NS results may not hold for high-order moments.

Our conclusive result here is that in a scalar field advected by 3D NS turbulence, the exponents $\zeta_p^\theta$ saturate to $\zeta_\infty^\theta$ at large orders and that the saturation exponent is connected to the fractal dimension of the steep fronts. We do not expect $\zeta_\infty^\theta$ to be universal, since $\zeta_p^\theta$ itself is non-universal [34, 56–58], but the fact that scalar exponents saturate in 3D NS flows can have important consequences. For instance, the minimum Hölder exponent of $\theta$, $h_{min}^\theta := \lim_{p\to\infty} \zeta_p^\theta/p = \lim_{p\to\infty} \zeta_\infty^\theta/p = 0$, implies that shock-like quasi-discontinuities, or steep fronts, characterize the large gradients of the scalar field, reminiscent of 1D Burgers flow. However, while the Burgers flow displays a bi-scaling behavior, the lower order scalar exponents appear to have a quadratic dependence on the order, similar to that derived for scalar advection in high-dimensional Kraichnan model [22]. This work sets the stage for similar investigations in the low ($Sc \ll 1$) and high ($Sc \gg 1$) Schmidt number regimes which have important physical applications [59–62]. We conjecture that the strong diffusion in the $Sc \ll 1$ limit may prevent such a saturation, whereas in the $Sc \gg 1$ case, the weak diffusion may enhance a saturation to the 1D Burgers limit. A careful analysis on the link between geometry and statistics in these two regimes is ongoing and will be reported as future work.

## ACKNOWLEDGMENTS

The computations and data analyses reported in this paper were performed using advanced computational facilities provided by the Texas Advanced Computation Center (TACC) under the XSEDE program supported by NSF. The data was generated using supercomputing resources at the Oak Ridge Leadership Computing Facility at the US Department of Energy Oak Ridge National Laboratory. The work of JS was supported by the Tandon School of Engineering at New York University and Grant No. SCHU 1410/19-1 of the Deutsche Forschungsgemeinschaft.

* kartik.iyer@nyu.edu

[1] S. T. Bramwell, P. C. W. Holdsworth, and J. F. Pinton, "Universality of rare fluctuations in turbulence and critical phenomena," Nature **396**, 552–554 (1998).
[2] R. Bruno and V. Carbone, "The solar wind as a turbulence laboratory," Living Rev. Sol. Phys. **10** (2013).
[3] S. F. Shandarin and Y. B. Zeldovich, "The large-scale structure of the universe: Turbulence, intermittency, structures in a self-gravitating medium," Rev. Mod. Phys. **61**, 185–220 (1989).
[4] A. Mashayek, R. Ferrari, S. Merrifield, J. R. Ledwell, S. L. Laurent, and A. N. Garabato, "Topographic enhancement of vertical turbulent mixing in the southern ocean," Nat. Commun. **8**, 14197 (2017).
[5] S. R. Tieszen, "On the fluid mechanics of fires," Annu. Rev. Fluid Mech. **33**, 67–92 (2001).
[6] A. S. Monin and A. M. Yaglom, *Statistical Fluid Mechanics*, Vol. 2 (MIT Press, 1975).

[7] B. I. Shraiman and E. D. Siggia, "Scalar turbulence," Nature **405**, 639–646 (2000).

[8] U. Frisch, *Turbulence* (Cambridge University Press, 1995).

[9] K. R. Sreenivasan and R. A. Antonia, "The phenomenology of small-scale turbulence," Annu. Rev. Fluid Mech. **29**, 435–472 (1997).

[10] K. R. Sreenivasan, "On local isotropy of passive scalars in turbulent shear flows," Proc. R. Soc. Lond. A **434**, 165–182 (1991).

[11] Z. Warhaft, "Passive scalars in turbulent flows," Annu. Rev. Fluid Mech. **32**, 203–240 (2000).

[12] S. Vernède, L. Ponson, and J. P. Bouchaud, "Turbulent fracture surfaces: A footprint of damage percolation?" Phys. Rev. Lett. **114**, 215501 (2015).

[13] S. Birkholz, E. T. J. Nibbering, C. Brée, S. Skupin, A. Demircan, G. Genty, and G. Steinmeyer, "Spatiotemporal rogue events in optical multiple filamentation," Phys. Rev. Lett. **111**, 243903 (2013).

[14] S. Drożdż, R. Gębarowski, L. Minati, P. Oświęcimka, and M. Watorek, "Bitcoin market route to maturity? evidence from return fluctuations, temporal correlations and multiscaling effects," Chaos **28**, 071101 (2018).

[15] J. P. Bouchaud, M. Mézard, and G. Parisi, "Scaling and intermittency in Burgers turbulence," Phys. Rev. E **52**, 3656–3675 (1995).

[16] D. Mitra, J. Bec, R. Pandit, and U. Frisch, "Is multiscaling an artifact in the stochastically forced Burgers equation?" Phys. Rev. Lett. **94**, 194501 (2005).

[17] J. Bec and K. Khanin, "Burgers turbulence," Phys. Rep. **447**, 1 – 66 (2007).

[18] R. H. Kraichnan, "Small-scale structure of a scalar field convected by turbulence," Phys. Fluids **11**, 945–953 (1968).

[19] R. H. Kraichnan, "Anomalous scaling of a randomly advected passive scalar," Phys. Rev. Lett. **72**, 1016–1019 (1994).

[20] V. Yakhot, "Passive scalar advected by a rapidly changing random velocity field: Probability density of scalar differences," Phys. Rev. E **55**, 329–336 (1997).

[21] M. Chertkov, "Instanton for random advection," Phys. Rev. E **55**, 2722–2735 (1997).

[22] E. Balkovsky and V. Lebedev, "Instanton for the Kraichnan passive scalar problem," Phys. Rev. E **58**, 5776–5795 (1998).

[23] A. Celani, A. Lanotte, A. Mazzino, and M. Vergassola, "Universality and saturation of intermittency in passive scalar turbulence," Phys. Rev. Lett. **84**, 2385–2388 (2000).

[24] G. Falkovich, K. Gawędzki, and M. Vergassola, "Particles and fields in fluid turbulence," Rev. Mod. Phys. **73**, 913–975 (2001).

[25] J. Kalda and A. Morozenko, "Turbulent mixing: the roots of intermittency," New J. Phys. **10**, 093003 (2008).

[26] R. A. Antonia, E. J. Hopfinger, Y. Gagne, and F. Anselmet, "Temperature structure functions in turbulent shear flows," Phys. Rev. A **30**, 2704–2707 (1984).

[27] C. Meneveau, K. R. Sreenivasan, P. Kailasnath, and M. S. Fan, "Joint multifractal measures: Theory and applications to turbulence," Phys. Rev. A **41**, 894–913 (1990).

[28] E. Lévêque, G. Ruiz-Chavarria, C. Baudet, and S. Ciliberto, "Scaling laws for the turbulent mixing of a passive scalar in the wake of a cylinder," Phys. Fluids **11**, 1869–1879 (1999).

[29] F. Moisy, H. Willaime, J. S. Andersen, and P. Tabeling, "Passive scalar intermittency in low temperature helium flows," Phys. Rev. Lett. **86**, 4827–4830 (2001).

[30] L. Skrbek, J. J. Niemela, K. R. Sreenivasan, and R. J. Donnelly, "Temperature structure functions in the Bolgiano regime of thermal convection," Phys. Rev. E **66**, 036303 (2002).

[31] T. Watanabe and T. Gotoh, "Statistics of a passive scalar in homogeneous turbulence," New J. Phys. **6**, 40 (2004).

[32] A. Gylfason and Z. Warhaft, "On higher order passive scalar structure functions in grid turbulence," Phys. Fluids **16**, 4012–4019 (2004).

[33] T. Watanabe and T. Gotoh, "Intermittency in passive scalar turbulence under the uniform mean scalar gradient," Phys. Fluids **18**, 058105 (2006).

[34] T. Gotoh and T. Watanabe, "Power and nonpower laws of passive scalar moments convected by isotropic turbulence," Phys. Rev. Lett. **115**, 114502 (2015).

[35] P. G. Mestayer, C. H. Gibson, M. F. Coantic, and A. S. Patel, "Local anisotropy in heated and cooled turbulent boundary layers," Phys. Fluids **19**, 1279–1287 (1976).

[36] C. H. Gibson, C. A. Friehe, and S. O. McConnell, "Structure of sheared turbulent fields," Phys. Fluids **20**, S156–S167 (1977).

[37] K. R. Sreenivasan, R. A. Antonia, and D. Britz, "Local isotropy and large structures in a heated turbulent jet," J. Fluid Mech. **94**, 745775 (1979).

[38] R. A. Antonia, A. J. Chambers, C. A. Friehe, and C. W. Van Atta, "Temperature ramps in the atmospheric surface layer," J. Atmos. Sci. **36**, 99–108 (1979).

[39] M. Holzer and E. D. Siggia, "Turbulent mixing of a passive scalar," Phys. Fluids **6**, 1820–1837 (1994).

[40] A. Pumir, "A numerical study of the mixing of a passive scalar in three dimensions in the presence of a mean gradient," Phys. Fluids **6**, 2118–2132 (1994).

[41] L. Mydlarski and Z. Warhaft, "Passive scalar statistics in high-Péclet-number grid turbulence," J. Fluid Mech. **358**, 135–175 (1998).

[42] D. A. Donzis and P. K. Yeung, "Resolution effects and scaling in numerical simulations of passive scalar mixing in turbulence," Physica D **239**, 1278–1287 (2010).

[43] P. K. Yeung, D. A. Donzis, and K. R. Sreenivasan, "Dissipation, enstrophy and pressure statistics in turbulence simulations at high Reynolds numbers," J. Fluid Mech. **700**, 5–15 (2012).

[44] K. P. Iyer and P. K. Yeung, "Structure functions and applicability of Yaglom's relation in passive-scalar turbulent mixing at low Schmidt numbers with uniform mean gradient," Phys. Fluids **26**, 085107 (2014).

[45] K. P. Iyer, K. R. Sreenivasan, and P. K. Yeung, "Refined similarity hypothesis using three-dimensional local averages," Phys. Rev. E **92**, 063024 (2015).

[46] S. Chen and R. H. Kraichnan, "Simulations of a randomly advected passive scalar field," Phys. Fluids **10**, 2867–2884 (1998).

[47] S. Chen and N. Cao, "Anomalous scaling and structure instability in three-dimensional passive scalar turbulence," Phys. Rev. Lett. **78**, 3459–3462 (1997).

[48] S. Kurien and K. R. Sreenivasan, "Measures of anisotropy and the universal properties of turbulence," (Springer Berlin Heidelberg, Berlin, Heidelberg, 2001) pp. 53–111.

[49] L. Biferale and I. Procaccia, "Anisotropy in turbulent flows and in turbulent transport," Phys. Rep. **414**, 43–

164 (2005).
[50] K. P. Iyer, F. Bonaccorso, L. Biferale, and F. Toschi, "Multiscale anisotropic fluctuations in sheared turbulence with multiple states," Phys. Rev. Fluids **2**, 052602 (2017).
[51] R. Benzi, S. Ciliberto, R. Tripiccione, C. Baudet, F. Massaioli, and S. Succi, "Extended self-similarity in turbulent flows," Phys. Rev. E **48**, R29–R32 (1993).
[52] G. Ruiz-Chavarria, C. Baudet, and S. Ciliberto, "Scaling laws and dissipation scale of a passive scalar in fully developed turbulence," Physica D **99**, 369 – 380 (1996).
[53] A. Celani, A. Lanotte, A. Mazzino, and M. Vergassola, "Fronts in passive scalar turbulence," Phys. Fluids **13**, 1768–1783 (2001).
[54] U. Frisch, A. Mazzino, and M. Vergassola, "Intermittency in passive scalar advection," Phys. Rev. Lett. **80**, 5532–5535 (1998).
[55] A. Mazzino and P. Muratore-Ginanneschi, "Passive scalar turbulence in high dimensions," Phys. Rev. E **63**, 015302 (2000).
[56] M. Chertkov, G. Falkovich, and V. Lebedev, "Nonuniversality of the scaling exponents of a passive scalar convected by a random flow," Phys. Rev. Lett. **76**, 3707–3710 (1996).
[57] B. I. Shraiman and E. D. Siggia, "Symmetry and scaling of turbulent mixing," Phys. Rev. Lett. **77**, 2463–2466 (1996).
[58] J. Lepore and L. Mydlarski, "Effect of the scalar injection mechanism on passive scalar structure functions in a turbulent flow," Phys. Rev. Lett. **103**, 034501 (2009).
[59] J. Schumacher and K. R. Sreenivasan, "Geometric features of the mixing of passive scalars at high schmidt numbers," Phys. Rev. Lett. **91**, 174501 (2003).
[60] L. P. Dasi, F. Schuerg, and D. R. Webster, "The geometric properties of high-schmidt-number passive scalar iso-surfaces in turbulent boundary layers," J. Fluid Mech. **588**, 253277 (2007).
[61] P. K. Yeung and K. R. Sreenivasan, "Direct numerical simulation of turbulent mixing at very low schmidt number with a uniform mean gradient," Phys. Fluids **26**, 015107 (2014).
[62] D. A. Donzis, K. Aditya, K. R. Sreenivasan, and P. K. Yeung, "The turbulent schmidt number," J. Fluids Eng. **136** (2014).